Int. J. Electrochem. Sci., 13 **(2018)** 8481 – 8495, doi: 10.20964/2018.09.12

International Journal of
ELECTROCHEMICAL
SCIENCE
www.electrochemsci.org

Enhanced Electrocatalytic Activity of Graphene-Gold Nanoparticles as a Superoxide Anion Biosensor Based on Immobilized Hemin

Beibei Wang [1], *Kai Kang*[1], *Xueping Ji* [1,2,*], *Yuheng Liu* [1], *Xianrui Li* [1], *Na Wang* [1], *Jujie Ren*[3,*]

[1] School of Pharmacy, Hebei Medical University, Shijiazhuang 050017, PR China
[2] Hebei Key Laboratory of Forensic Medicine, Shijiazhuang 050017, PR China
[3] Department of Chemistry, School of Sciences, Hebei University of Science and Technology, Shijiazhuang 050018, PR China
[*]E-mail: xuepingji@126.com, xpji03@yahoo.com.cn, jujieren@126.com

Received: 4 April 2018 / *Accepted:* 25 May 2018 / *Published:* 5 August 2018

Inspired by the high electrocatalytic activity of electrochemically reduced graphene oxide-Au nanoparticles (ERGO-AuNPs) nanohybrid and their strong adsorption capacity for immobilizing biomolecules, we developed an ultrasensitive superoxide anion ($O_2^{\bullet-}$) electrochemical biosensor based on hemin immobilized on ERGO-AuNPs nanohybrid modified glass carbon electrode (GCE). The electrochemical properties of immobilized hemin were investigated. A considerably higher surface concentration (Γ^*) of the immobilized hemin was measured on the order of 1.02×10^{-7} mol cm^{-2}. The results indicated that the ERGO-AuNPs nanohybrid enhanced the electrocatalytic activity of hemin for $O_2^{\bullet-}$ detection due to the synergy generated by ERGO and AuNPs. The resulting biosensor exhibited an excellent amperometric response toward $O_2^{\bullet-}$, at linear ranges of 3.28×10^{-5} to 3.28×10^{-4} M with sensitivities of 186 nA $\mu M^{-1}cm^{-2}$ and 124 nA $\mu M^{-1}cm^{-2}$ at 0.5 V and −0.1 V, separately. The apparent Michaelis–Menten constant (K_m) was estimated to be 0.51 mM and 0.48 mM at 0.5 V and −0.1 V, respectively, which indicated a clearly stronger interaction of hemin with $O_2^{\bullet-}$. The results indicated that the biosensor have strong potential for analysis of biological molecules.

Keywords: Superoxide anion, Electrochemical reduced graphene oxide, Au nanoparticles, Nanohybrid, Biosensor

1. INTRODUCTION

Superoxide anion ($O_2^{\bullet-}$), one of the most abundant reactive oxygen species (ROS), has been recognized as being involved in many physiological and pathological processes [1-4]. The normal

amount of superoxide anion is beneficial for immune response, but due to its instability, it could also contribute to oxidative stress by generating a cascade of reactive oxygen species. Such oxidative stress could produce damage to lipids, proteins or DNA, thereby impeding normal cell functions. Therefore, the exact determination of $O_2^{\bullet-}$ in vivo is very important in understanding the role which $O_2^{\bullet-}$ plays in pathology and physiology.

Conventionally, the detection and quantitation of $O_2^{\bullet-}$ include conductometric analysis, EPR spectroscopy, or by certain semi-quantitative colorimetric tests [5-8]. However, these methods are costly, complex, and have poor specificity, thereby restricting their use in biological systems. Electrochemical sensors have been explored for free radical detection in recent years due to their substrate specificity and higher turnover rates [9]. There are two main types of electrochemical superoxide sensors. One type is developed based on superoxide dismutase (SOD) [10-12]. In this case, SOD can catalyze the dismutation of the $O_2^{\bullet-}$ to O_2 and H_2O_2 efficiently and specifically but serious interference appears in the medium at high electrode potential of 0.5 V (vs. Ag/AgCl), which limits the application in physiological systems. To eliminate electroactive interferences, permeable membranes, such as Teflon, have been employed to modify the electrodes [13]. However, the sensitivity and the response rate are comparatively decreased. The other type of sensor is based on cytochrome c (cyt c) [14-16]. Analytical applications of cyt c for electrochemical assay of superoxide is developed on the metal center (Fe(III)/Fe(II)) in cyt c molecules, which leads to a current proportional to the superoxide concentration. However, the reproducibility and stability of this type of sensor are unsatisfactory because of the relatively low reusability and poor operational stability of the cyt c on the electrode.

Hemin is a well-known natural metalloporphyrin, and the active center of the heme-protein family can catalyze the reduction of many important analytes, such as oxygen, nitrite, nitric oxide, trichloroacetic acid, l-cystein and superoxide anion based on the reversible redox of Fe(III)/Fe(II) [17-19]. Recently, it has been shown that hemin possess high catalytic activity and stability on carbon electrodes, especially on graphene modified electrodes. Therefore, it is promising technique to characterize the function of graphene with hemin towards the development of novel superoxide sensors.

Graphene, a two-dimensional monolayer of graphite, has good electroactivity, large surface area, good biocompatibility and high mobility of charge carriers [20,21] and has been applied in lithium ion batteries [22], super-capacitors [23], and chemical and biosensors [24,25]. Moreover, recent research has demonstrated that a combination of graphene with other nanomaterials can been developed into a preferred material, which exhibits the merits of both components [26,27]. Especially, graphene functionalized with metal nanoparticles have been of particular interest due to their excellent electrocatalytic activity and better synergistic properties [28-30]. In our previous study, we developed a new way to create a density controllable, highly sensitive electrochemically reduced graphene oxide (ERGO)-AuNPs nanohybrid. It was found that the ERGO-AuNPs nanohybrid exhibited remarkable electrochemical properties [31,32] and exhibited strong potential in enhancing the electrocatalytic activity of a biosensor. Based on that finding, this paper describes the characterization and application

of a superoxide biosensor that was prepared by immobilizing hemin on ERGO-AuNPs nanohybrid. The results suggested that the immobilized hemin showed promising electrocatalytic activity with regard to $O_2^{\bullet-}$, and it could thus be used as a sensitive reagentless biosensor for $O_2^{\bullet-}$.

2. EXPERIMENTAL

2.1. Materials and chemicals

Graphite powder was provided by Sinopharm Chemical Reagent Co. Ltd. (China). Chitosan (CS, MW 1.5×10^5, 75%–85% deacetylation) was obtained from Yuhuan Chemical Factory (Zhejiang, China). Iron protoporphyrin IX (hemin, from Porcine), Potassium dioxide (KO_2) and chloroauric acid trihydrate ($HAuCl_4\cdot3H_2O$) obtained from Sigma, were used without further purification. Potassium ferricyanide was the product of Shanghai Chemical Reagent Factory (Shanghai, China). All other chemicals were of analytical reagent grade, and used as received.

Graphite oxide (GO) was synthesized from graphite powder using the method outlined by Hummers and Offeman method [33], and it was characterized using the UV-Vis absorption spectra. The obtained aqueous dispersion of GO sheet (2 mg mL^{-1}) was stored at 4 ℃ for further use.

A stock solution of superoxide ion ($O_2^{\bullet-}$) was prepared by adding KO_2 to dimethyl sulfoxide (stored together with molecular sieve 4 ˚A) and sonicating the solution for 30 min [34]. The stock solutions were stored at 4 ℃. The $O_2^{\bullet-}$ concentration from the absorption intensity of $O_2^{\bullet-}$ at 260 nm using a molar absorptivity of $O_2^{\bullet-}$ at 260 nm, ε_{260} = 1350 $mol^{-1}cm^{-1}$ [35].

2.2. Apparatus

Electrochemical measurements were performed on an electrochemical analyzer (CHI 852D, Shanghai, China) at ambient temperature (23±2 ℃) in an aqueous solution containing 0.1 M PBS with a three-electrode configuration, in which bare GC and modified electrodes were used as the working electrodes, a Pt wire was used as the counter electrode and an Ag/AgCl (3 M KCl) electrode was used as reference electrode. A UV-Vis spectrophotometer (TU-1901, Beijing, China) was applied for the characterization of GO and the evaluation of $O_2^{\bullet-}$ concentration.

2.3. Preparation of the modified electrode

The modified electrodes were prepared in the same way as reported in the previous paper [9]. Briefly, the GCE (3 mm Φ) was cleared, and an aliquot of 15 μL GO aqueous dispersion was cast on the top of the GCE and dried in air. Next, one-step electrochemical deposition of ERGO-AuNPs was

conducted using potentiostatic deposition onto the GCE in a stirred 0.10 M PBS containing 1.25 mM $HAuCl_4$. The applied deposition potential was fixed at −1.4 V, and the deposition time was 720 s. Next, 5 μL of 6.0 mM hemin was cast onto the surface of the ERGO-AuNPs/GCE and nearly dried in a refrigerator at 4 ℃. Finally, an aliquot of 5 μL 1% CS solution was dropped onto the surface of the hemin/ERGO-AuNPs/GCE and nearly dried. The resulting CS/hemin/ERGO-AuNPs/GCE was thoroughly washed with water and stored in 0.10 M PBS (pH 7.0) at 4℃ for future use.

3. RESULTS AND DISCUSSION

3.1. Characterization of ERGO-AuNPs nanohybrid

The morphology and electrochemical behavior of the ERGO-AuNPs nanohybrid modified GCE were investigated using scanning electron microscope (SEM) and cyclic voltammetry (CV), as they were in our previous study [9]. SEM images showed that AuNPs were deposited onto the ERGO sheet structure, creating a considerably rougher ERGO-AuNPs nanohybrid (as shown in Fig. 1(A), which greatly increased the surface area of the electrode and provided a conductive pathway for electron transfer. The SEM images of the ERGO and AuNPs modified electrode are shown in Supplementary Information (Fig. S1). Electrochemical studies of the modified electrodes showed that the peak currents of ERGO-AuNPs/GCE (Fig. 1(B), curve c) are considerably higher (ca 2 times) than that of the AuNPs/GCE (Fig. 1(B), curve b) or ERGO/GCE (Fig. 1(B), curve a) in 0.10 M PBS containing 5 mM $[Fe(CN)_6]^{3-/4-}$.

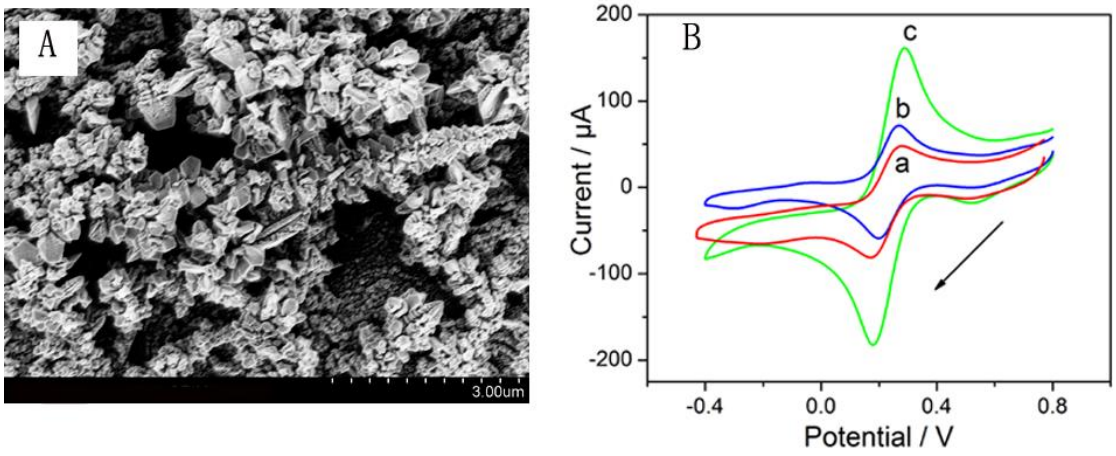

Figure 1. (A) SEM images of ERGO-AuNPs film. (B) CVs obtained from different modified electrodes in 0.10 M PBS containing 5 mM $[Fe(CN)6]^{3-/4-}$ at a scan rate of 20 mV s^{-1}. (a) AuNPs/GCE, (b) ERGO/GCE, (c) ERGO-AuNPs/GCE.

The results indicated that the one-step co-electrochemical deposition of ERGO and AuNPs onto the electrode could greatly amplify electrochemical response compared to the electrodeposition of metal nanoparticles on the reduced graphene oxide [36]. The reason for this finding might be that the synergy generated by ERGO and AuNPs could result in enhanced conductivity and improved charge transfer rates between the redox probe and the modified electrode surface.

3.2. Electrochemistry of the hemin immobilized on ERGO-AuNPs nanohybrid

The electrochemical behavior of the immobilized hemin was investigated by CV in our previous study [9]. The formal potential ($E^{0'}$), taken as the average of cathodic peak potential (E_{pc}) and anodic peak potential (E_{pa}), was −0.35 V (*vs.* Ag/AgCl (3 M KCl)), with ΔE_p, the peak-to-peak potential separation of anodic and cathodic waves, 0.085 V at a scan rate of 20 mV s^{-1}, as shown in Fig. 2. The redox peak currents (the ratio of the anodic and cathodic peak currents was close to 1.0) were directly proportional to the potential scan rates at low scan rates, showing the characteristic of a typical surface adsorption controlled process.

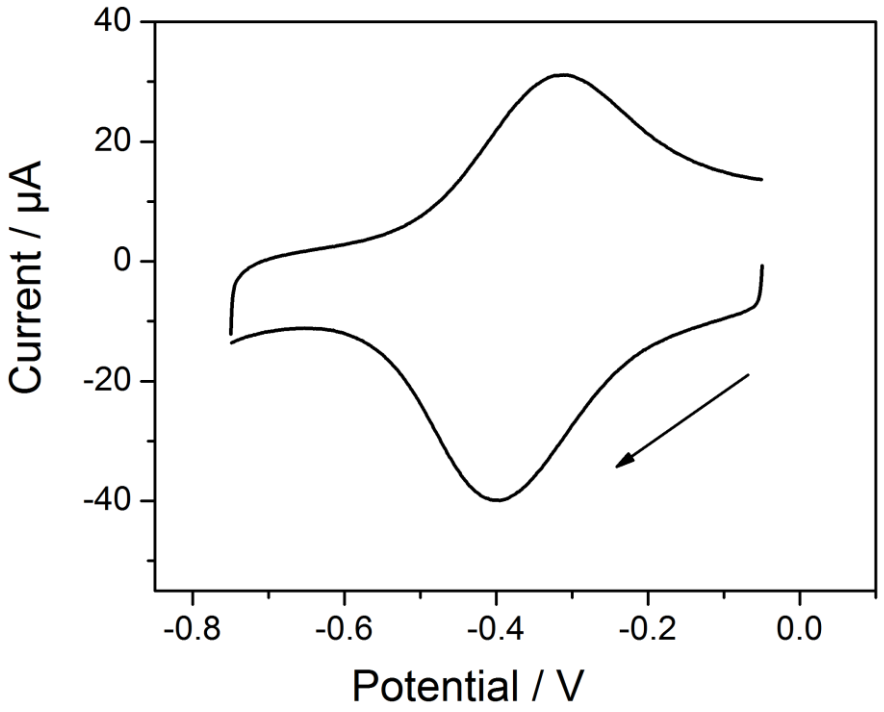

Figure 2. CVs obtained from hemin/ERGO-AuNPs/GCE in 0.10 M PBS at a scan rate of 20 mV s^{-1}.

In the present study, the surface concentration (Γ^*) of the immobilized hemin on ERGO-AuNPs nanohybrid was estimated by integration of the CV reduction peaks with the formula $Q=nFA\Gamma^*$, where Q is the charge involved in the reaction, n is the number of electrons transferred, F is

the Faraday constant, and *A* is the geometric area of the electrode. By integrating the reduction peak currents, the surface coverage of the electroactive hemin was calculated as 1.02×10^{-7} mol cm^{-2}, which was much larger than that reported for hemin-carbon nanomaterial films (7.8×10^{-9} mol cm^{-2}) and hemin-pyrolytic graphite (7.45×10^{-9} mol cm^{-2}) [37,38]. The results suggested that the presence of the ERGO-AuNPs nanohybrid film with a large effective surface area helped to increase the adsorption of hemin. This finding was attributable to the hemin that could be strongly absorbed on the surface of ERGO-AuNPs nanohybrid through π-π stacking interactions, which could effectively decrease the agglomeration of hemin, leading to a considerably higher exposed surface area. Conversely, the synergy generated by ERGO and AuNPs accelerated the electron transfer between hemin and the electrode and significantly improved the electrochemical response.

3.3. Electrochemical response of CS/hemin/ERGO-AuNPs/GCE toward superoxide ion

The responses of $O_2^{\bullet-}$ on the modified electrode were evaluated by differential pulse voltammetry (DPV) in 0.1 M PBS in the potential range from −0.7 and −0.2 V (shown in Fig. 3). Clearly, the successive addition of $O_2^{\bullet-}$ into the electrolyte solution led to the continuous increase of the cathodic peak current of ca. −0.4 V, which could be attributed to the electrocatalysis of hemin. As shown in Scheme. 1, the mechanism for the electrochemical catalytic oxidation of $O_2^{\bullet-}$ is based on the redox reaction of hemin (Fe^{3+}/ Fe^{2+}). Upon the addition of $O_2^{\bullet-}$ into the buffer solution, the reduction of hemin (Fe^{3+}) to hemin (Fe^{2+}) occurred, and the reoxidation of hemin (Fe^{2+}) to hemin (Fe^{3+}) occurred at the surface of the modified electrode by direct electron transfer. The current generated at the electrode is proportional to the $O_2^{\bullet-}$ concentration.

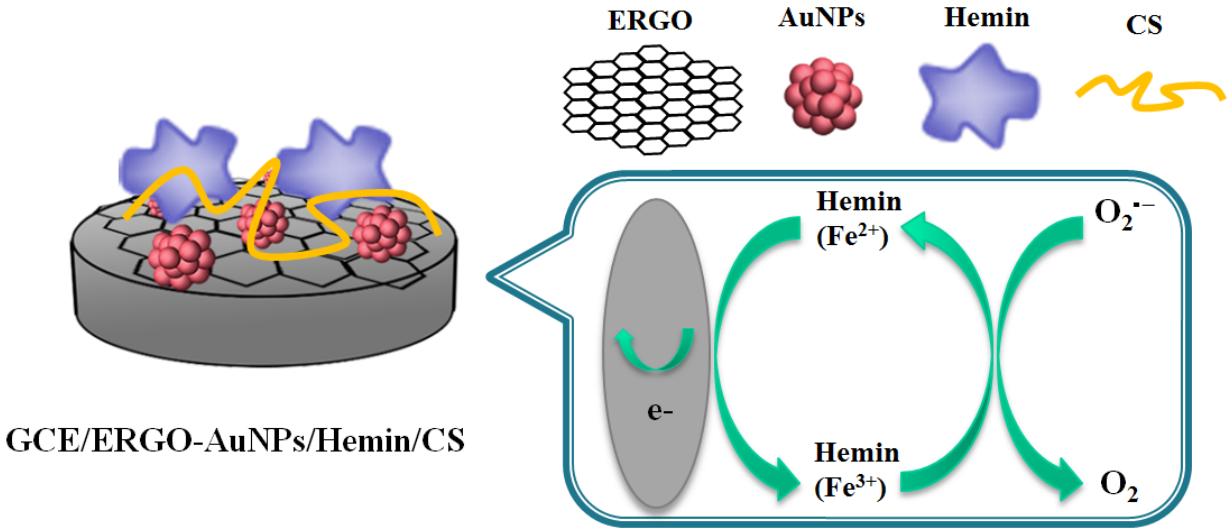

Scheme 1. Schematic illustration of the mechanism for the electrochemical catalytic reaction.

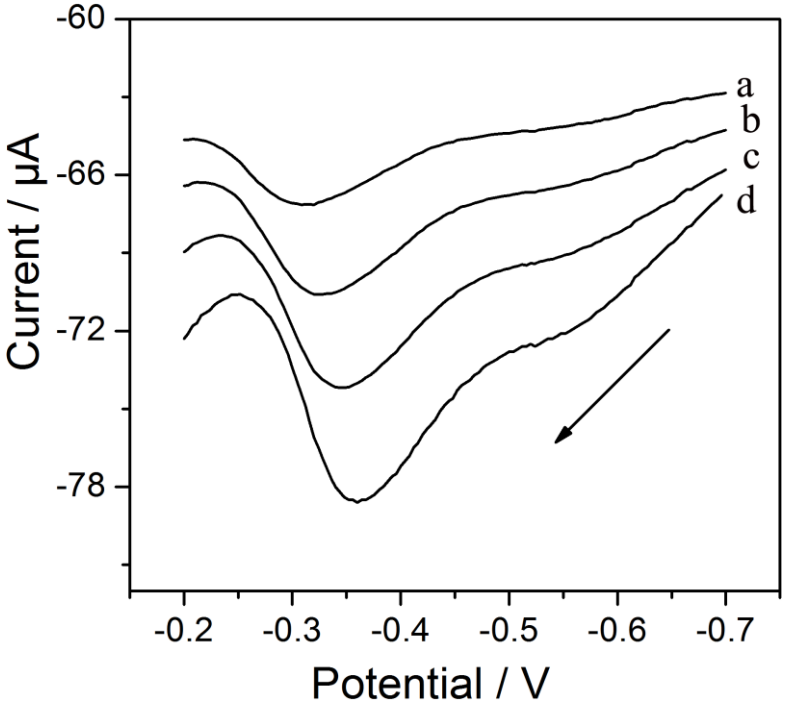

Figure 3. DPV obtained at CS/hemin/ERGO-AuNPs/GCE in 0.10 M PBS (pH 7.0) from different concentrations of $O_2^{\bullet-}$ (a-d: 0, 50, 75, 100 μM).

3.4. Enhancement effect of ERGO-AuNPs toward superoxide ion catalysis

To study the catalytic activity of hemin in different modified materials, electrodes with different modifications were prepared. Fig. 4 displays the CVs of 75 μM $O_2^{\bullet-}$ in a pH 7.0 buffer solution at different modified electrodes. Both the cathodic peak currents of CS/hemin/AuNPs/GCE (Fig. 4(A)), CS/hemin/ERGO/GCE (Fig. 4(B)) and CS/hemin/ERGO-AuNPs/GCE (Fig. 4(C)) obviously increased with the addition of 75 μM $O_2^{\bullet-}$ into solution, while for the CS/hemin/AuNPs/GCE (Fig. 4(A)) and CS/hemin/ERGO/GCE (Fig. 4(B)), the increase of the cathodic peak currents of $O_2^{\bullet-}$ were calculated as I_{pc} =5.0×10^{-7} μA and I_{pc} =6.2×10^{-7} μA, respectively, which can be ascribed to the catalytic reactions of $O_2^{\bullet-}$ at the ERGO and AuNPs modified electrode. However, the CS/hemin/ERGO-AuNPs/GCE (Fig. 4(C)) shows a distinct increase of the cathodic peak currents (I_{pc} = 25.68×10^{-7} μA), which were approximately five times more than that of CS/hemin/AuNPs/GCE and CS/hemin/ERGO/GCE. This amplified electrochemical response indicated that the combination of ERGO with AuNPs effectively accelerated the electrocatalytic activity of hemin for $O_2^{\bullet-}$ detection, which was attributed to the synergy produced by ERGO and AuNPs incorporated in the nanohybrid that greatly promoted electron transfer in the sensing interface [9,32].

At the same time, the adsorption of hemin largely increased on the ERGO-AuNPs nanohybrid due to the expansion of the conductive area of the nanohybrid film. Additionally, the stability of hemin was also enhanced on the ERGO-AuNPs nanohybrid film through π-π interactions. According to the result, it could be confirmed that the proposed nanohybrid is a good platform for electrochemical sensing applications.

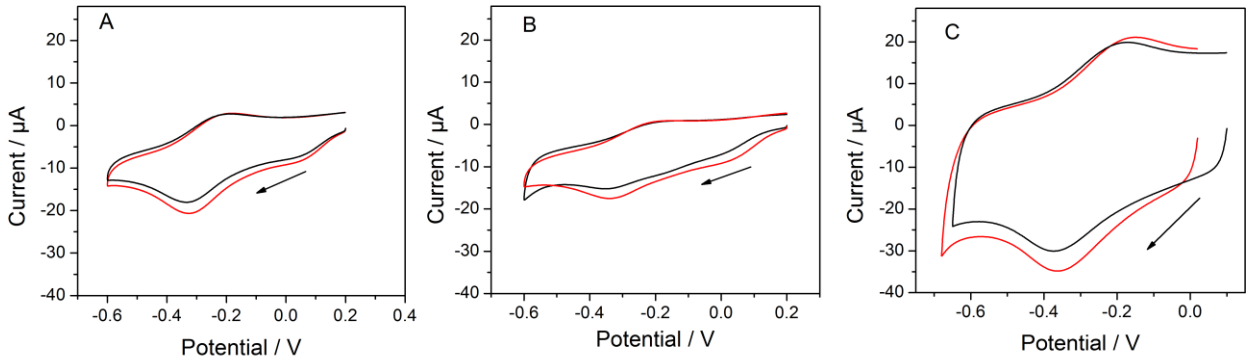

Figure 4. CVs at CS/hemin/AuNPs/GCE (A), CS/hemin/ERGO/GCE (B) and CS/hemin/ERGO-AuNPs/GCE (C) in 0.10 M PBS (pH 7.0) in the absence (black) and in the presence (red) of 75 μM $O_2^{\bullet-}$. Potential scan rate: 20 mV s^{-1}.

3.5. Effect of applied potential and solution pH on the biosensor response

Applied potential is an important effect factor on the selectivity and sensitivity of the biosensor. Thus, before performing a calibration plot for $O_2^{\bullet-}$, a hydrodynamic voltammetric study (Fig. 5) was also performed at CS/hemin/ERGO-AuNPs/GCE, in the potential window ranging from −0.6 to 0.7 V (vs. Ag/AgCl) in 0.1 M PBS containing 75 μM $O_2^{\bullet-}$. As shown in Fig. 5, the response current reached a maximum value at −0.1 V in the reduction range, which is similar to the case of the sol-gel modified electrode for the detection of $O_2^{\bullet-}$ at 0.0 V [39] and the hemin modified sonogel–carbon electrode for the detection of $O_2^{\bullet-}$ at −0.15 V [40]. After that step, the response current decreased as the applied potential continued to increase. However, when the applied potential increased from 0.2 to 0.7 V, the response current increased again and reached another maximum at 0.5 V. This result is similar to the case of the biosensors based on SOD modification [41].

The pH of the solution affects both the hemin activity and the substrate's electron transfer. Fig. 6 shows the elctrochemical response of the biosensor (measured in 0.1 M PBS (pH 5.0 to 9.0) containing 75 μM $O_2^{\bullet-}$) increased at first with increasing pH of the solution and later decreased as the pH changed from 7.0 to 9.0; therefore, the maximum response was obtained at pH 7.0. Considering the sensitivity of the biosensor and the practical biosensing applications, the PBS of pH 7.0 was selected as the optimal supporting electrolyte.

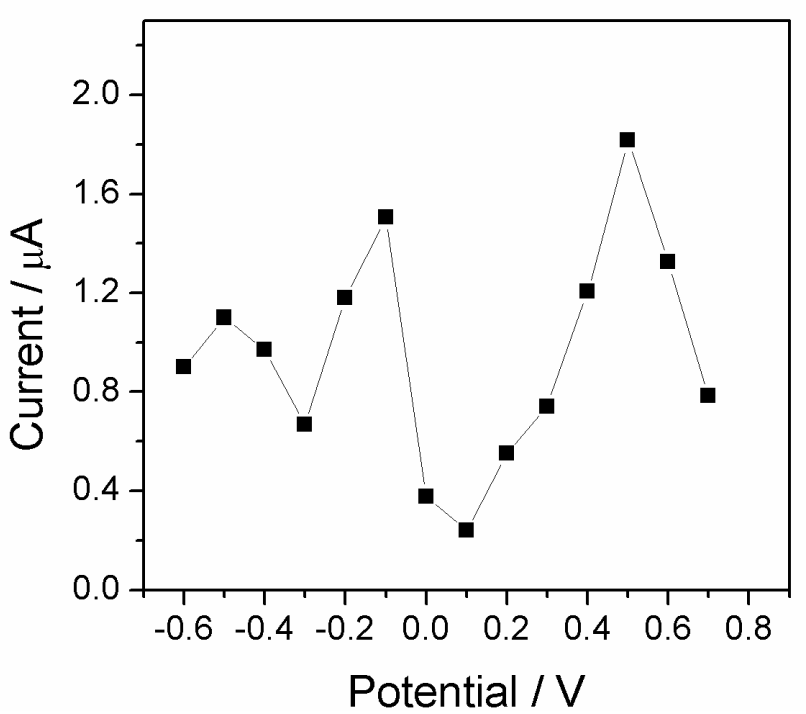

Figure 5. Effect of applied potential on the response current of the CS/hemin/ERGO-AuNPs/GCE in 0.1 M PBS containing 75 μM $O_2^{\bullet-}$.

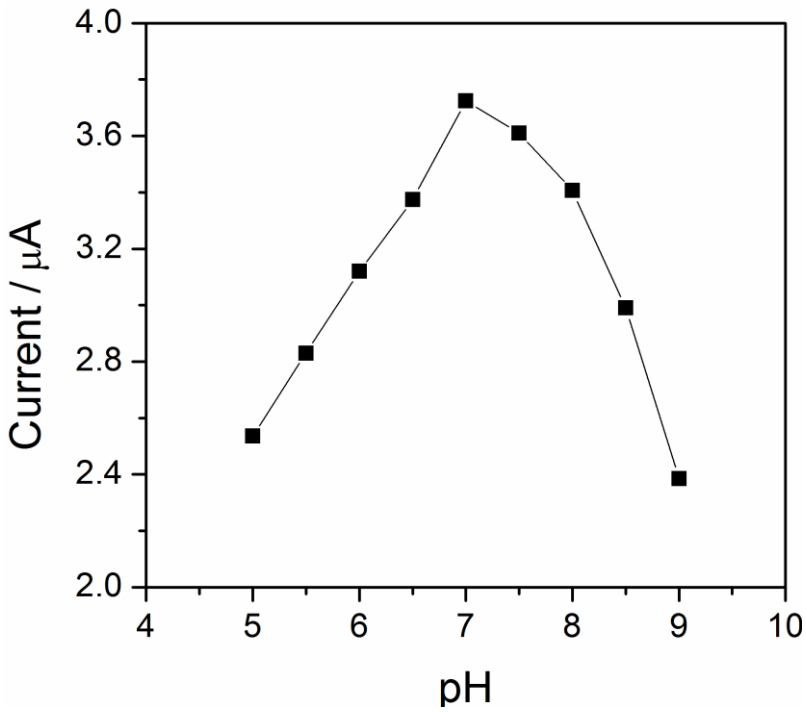

Figure 6. Effect of pH on the response current of the CS/hemin/ERGO-AuNPs/GCE in 0.1 M PBS containing 75 μM $O_2^{\bullet-}$.

3.6. Amperometric response of the biosensor towards $O_2^{\bullet-}$

Under the optimum conditions, an amperometric i-t curve (*I-T*) was used to detect $O_2^{\bullet-}$ at the modified electrode. Fig. 7 (A) illustrated the responses of the modified electrode at the applied potentials of +0.5 V (curve a) and −0.1 V (curve b) (vs. Ag|AgCl). Well-defined steady-state current responses of the biosensor were proportional to the increasing concentrations of $O_2^{\bullet-}$ in the range of 3.28×10^{-5} to 3.28×10^{-4} M (Fig. 7(B)), with detection limits of 2.0 μM and 3.0 μM, at 0.5 V and −0.1 V, respectively. From the slope (13.62 $nA\mu M^{-1}$ and 8.829 $nA\mu M^{-1}$) of the calibration curves, sensitivities of 186 $nA\mu M^{-1}cm^{-2}$ and 124 $nA\mu M^{-1}cm^{-2}$ were obtained. The comparison of the resulting biosensor with other reported $O_2^{\bullet-}$ biosensors is shown in Table 1. This finding indicates the sensitivity of the biosensor was 30 times higher than that of the previously reported results of 4.0 $nA\mu M^{-1}cm^{-2}$ on an SOD/nano Fe_3O_4-modified gold electrode [41] and 156 times higher than that of 0.782 $nA\mu M^{-1}cm^{-2}$ on an SOD/sol-gel modified gold electrode [39]. The results above demonstrated that the introduction of ERGO-AuNPs nanohybrid dramatically enhanced the electrochemical response of the resulting electrode to $O_2^{\bullet-}$. This finding may be ascribed to the synergistic effects of ERGO-AuNPs, which can not only provide higher efficient diffusion pathways for the electrolyte ions and produce signal amplification in electrochemical detection but can increase the surface adsorption of hemin and provide a favorable microenvironment for excellent catalytic activity of hemin on the area of graphene nanosheets due to the high surface area of ERGO and AuNPs and good biocompatibility. In addition, with a further increase in $O_2^{\bullet-}$ concentration, the reaction process follows the conventional enzymatic dynamic regulation of the Michiaelis–Menten equation. The apparent Michaelis-Menten constant (*K*m) could be calculated as 0.51 mM and 0.48 mM from the Lineweaver-Burk equation, which were smaller than a polymerized hemin-modified GCE (*K*m =0.7 mM) [44]. The relatively small *K*m values indicate that the affinity between $O_2^{\bullet-}$ and the hemin is stronger than that of polymerized hemin.

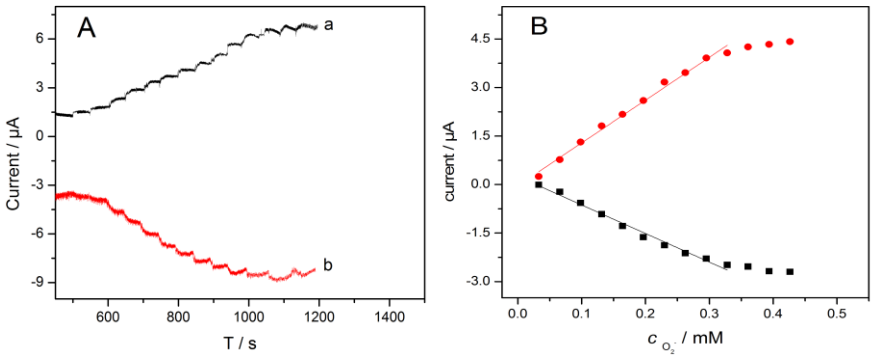

Figure 7. (A) Typical amperometric curves at CS/hemin/ERGO-AuNPs/GCE for successive addition of $O_2^{\bullet-}$ in 0.1 M PBS (pH 7.0) at the applied potentials of (a) +0.5 V and (b) −0.1 V (vs. Ag|AgCl). (B) Plots of amperometric responses upon the addition of $O_2^{\bullet-}$ in 0.1 M PBS (pH 7.0) at the applied potential of (a) +0.5 V and (b) −0.1 V (vs. Ag|AgCl).

3.7. Anti-interference ability of the biosensor

To evaluate the selectivity of biosensor, several potential sources of interference, including uric acid (UA), L-cystine, NO_2^-, dopamine (DA), NO_3^-, H_2O_2 and glucose (Glu), were examined. It was found that the selectivity of biosensor is potential dependent. As illustrated in Fig. 8, the negligible response for potential interferences appeared at −0.1 V (bar green), in contrast to the response at +0.5 V (bar red), suggesting higher selectivity of the biosensor for $O_2^{\bullet-}$ at −0.1 V (bar green). The result is consistent with the case of the superoxide biosensors based on SOD, which has higher selectivity at the low electrode potential [43]. The reason for this finding might be that electroactive interference could be co-oxidized at the high potential. However, that no obvious response current of interference was observed, except in the case of H_2O_2, in contrast to the large response to $O_2^{\bullet-}$ both at +0.5 V (bar red) and −0.1 V (bar green). This finding is due to the use of CS, which can restrain electroactive interference from permeating into the film, caused CS/hemin/ERGO-AuNPs/GCE to exhibit little or no response for the interfering species DA and UA, thereby causing CS/hemin/ERGO-AuNPs/GCE to have a good selectivity. The inference from H_2O_2 could be basically eliminated by the addition of 2 U/mL catalase enzyme to the reaction media.

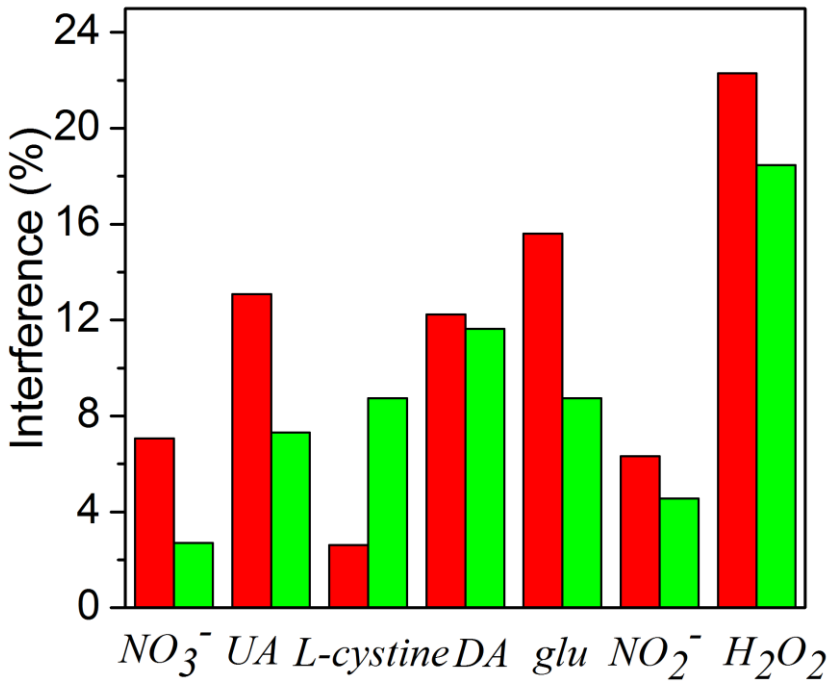

Figure 8. Typical selectivity profile of CS/hemin/ERGO-AuNPs/GCE obtained at different applied potentials: −0.1 V (bar green) and 0.5 V (bar red) (vs. Ag|AgCl) toward addition of Glu, DA, NO_2^-, UA, L-cystine, H_2O_2 and NO_3^-. (NO_3^-, UA, L-cystine, NO_2^-: 100 μM; DA, H_2O_2: 50μM and Glu: 1 mM. All of the interferences are compared to 50 μM $O_2^{\bullet-}$.

3.8. Stability of the biosensor

The shelf life of the CS/hemin/ERGO-AuNPs/GCE bioelectrode was investigated by detecting electrochemical response for two weeks. The experimental results showed the electrochemical signal could retain approximately 80% of its initial response to $O_2^{\bullet-}$ when stored in a phosphate buffer solution ((0.1 M PBS of pH 7.0 at 4℃).

Table 1. Comparison of the performances of proposal sensor for the detection of $O_2^{\bullet-}$ with those of sensors based on different matrices

Electrode	Linear range (μM)	Sensitivity ($nA\mu M^{-1}cm^{-2}$)	Detection limit (μM)	Ref.
CS/hemin/ERGO-AuNPs/GCE	32.8–328	186, 124	0.2, 0.3	This work
SOD/nano Fe_3O_4/Au	0.2–1.4	4.0	0.003	41
SOD/SA/Au	0.44–229.88	0.782	0.23	39
PMMA/PANI–Au_{nano}/SOD–ITO	0.5-2.4	42.5	0.3	42
Mn-SOD/MPA/GCE	74.5–725.4, 96.8–1020	7.1 ± 0.3, 8.8 ± 1.2	8.3, 9.1	43

SOD: superoxide dismutases

nano Fe_3O_4: iron oxide nanoparticles

SA: sodium alginate

PMMA: poly(methyl methacrylate)

PANI: polyaniline

Au_{nano}: gold nanoparticles

ITO: indium-doped tin oxide

MPA: 3-mercaptopropionic acid

4. CONCLUSIONS

In the present work, a novel biosensor was successfully fabricated for the sensitive and rapid detection of $O_2^{\bullet-}$ based on immobilizing hemin on a density controllable ERGO-AuNPs nanohybrid. The combination of ERGO with AuNPs co-electrodeposited on GCE played an important role for the inhibition of the aggregation of hemin through π-π stacking interactions of hemin with ERGO, resulting in enhanced hemin adsorption. Moreover, the ERGO-AuNPs nanohybrid provided an

increase in the effective surface area of the electrode, as well as accelerating the electron transfer rate on the electrode interface due to its synergistic effects. Under the optimal experimental conditions, the constructed biosensor exhibited a satisfactory linear range, high sensitivity, excellent reproducibility, storage stability and good selectivity towards $O_2^{\bullet-}$ determination.

SUPPLEMENTARY INFORMATION:

The ERGO film electrodeposited on the GCE clearly showed a large, sheet-like shape, which was the typical stacks of wrinkled multilayer graphene (Fig. S1(A)). As shown in Fig. S1(B), the AuNPs have a spherical shape with a size of approximately 50–100 nm.

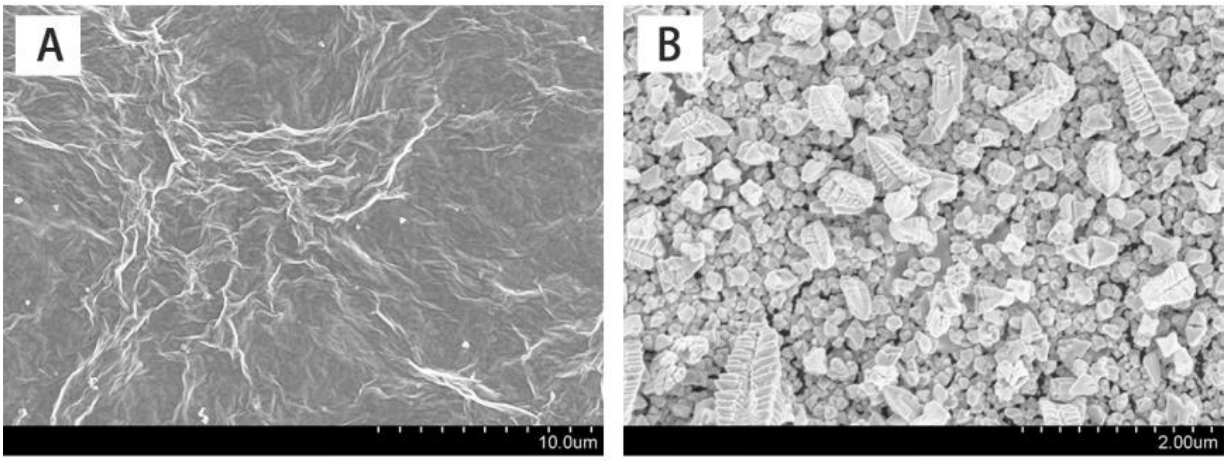

Figure S1. SEM images of ERGO film (A), AuNPs film (B).

ACKNOWLEDGMENTS

This work was financially supported by the Natural Science Foundation of Hebei Province of China (No. B2016206150) and the Scientific Research Projects of Hebei Province Department of Education (No. ZD2018037 and No. ZC2016069).

References

1. P. Kachroo, G. Lim and A. Kachroo, *Adv. Bot. Res*., 77 (2016) 245.
2. S. Li, H. Tan, N. Wang, Z. Zhang, L. Lao, C. Wong and Y. Feng, *Int. J. Mol. Sci*., 16 (2015) 26087.
3. D. Lu, L. Zhou, R. Wang, X. B. Zhang, L. He, J. Zhang and W. Tan, *Sens. Actuator B*, 250 (2017) 259.
4. H. Xiao, X. Liu, C. Wu, Y. Wu, P. Li, X. Guo and B. Tang, *Biosens. Bioelectron*., 91 (2017) 449.
5. A. Nishino, T. Maoka and H. Yasui, *Tetrahedron Lett.*, 57 (2016) 1967.
6. L. L. Bronsart, C. Stokes and C. H. Contag, *Mol. Imaging. Biol*., 18 (2016) 166.
7. A. K. Poulsen, A. M. Scharff-Poulsen and L. F. Olsen, *Anal. Biochem.*, 366 (2007) 29.

8. H. D. Wang, P. J. Pagano, Y. Du, A. J. Cayatte, M. T. Quinn, P. Brecher and A. C. Richard, *Circ. Res.*, 82 (1998) 810.
9. B. Wang, X. Ji, J. Ren, R. Ni and L. Wang, *Bioelectrochemistry*, 118 (2017) 75.
10. S. Mesaros, Z. Vankova, S. Grunfeld, A. Mesarosova and T. Malinski, *Anal. Chim. Acta*., 358 (1998) 27.
11. V. Lvovich and A. Scheeline, *Anal. Chem*., 69 (1997) 454.
12. F. Peng, T. Xu, F. Wu, C. Ma, Y. Liu, J. Li and C. Mao, *Talanta*, 174 (2017) 82.
13. M. I. Song, F. F. Bier and F. W. Scheller, *Bioelectrochem. Bioenerg.*, 38 (1995) 419.
14. Y. Luo, T. Yang, A. Zhu, H. Liu and J. Zhou, *J. Electroanal. Chem.*, 642 (2010) 109.
15. X. Ji, J. Ren, J. Jin and T. Nakamura, *Biosens. Bioelectron.*, 23 (2007) 241.
16. C. M. Tolias, J. C. McNeil, J. Kazlauskate and E. W. Hillhouse, *Free Radical Biol. Med.*, 26 (1999) 99.
17. W. J. R. Santo, P. R. Lima, C. R. T. Tarley, N. F. Hoehr and L. T. Kubota, *Anal. Chim. Acta.*, 631 (2009) 170
18. Y. Zhang, Z. Xia, H. Liu, M. Yang, L. Lin and Q. Li, *Sens. Actuator B*, 188 (2013) 496.
19. Y. Liu, Y. L. Yan, J. Lei, F. Wu and H. X. Ju, *Electrochem. Commun.*, 9 (2007) 2564.
20. S. Li, H. Tan, N. Wang, Z. Zhang, L. Lao, C. Wong, and Y. Feng, *Int. J. Mol. Sci.*, 16 (2015) 26087.
21. P. Kovacic and J. D. Jacintho, *Curr. Med. Chem*.8 (2001) 773.
22. J. Zhou, Y. Luo, A. Zhu, Y. Liu, Z. Zhu and Y. Tian, *Analyst* 136 (2001)1594.
23. D. Tsikas, *Analyst* 136 (2011) 979.
24. E. Cakmak, S. Yardim-Akaydin, E. Caliskan-Can, H. Firat and S. Ardic, *Oxid.Commun*. 38 (2015) 2064.
25. F. Bedioui, D. Quinton, S. Griveau and T. Nyokongc, *Phys. Chem. Chem. Phys.* 12 (2010) 9976.
26. Y. Zhu, D. Pan, X. Hu, H. Han, M. Lin and C. Wang, *Sens. Actuator B*, 243 (2017) 1.
27. J. Li, J. Xie, L. Gao and C. M. Li, *ACS Appl. Mater. Interfaces*, 4 (2015) 2726.
28. H. Cong, X. Ren, P. Wang and S. Yu, *ACS Nano*, 3 (2012) 2693.
29. N. Shams, H. N. Lim, R. Hajian, N. A. Yusof, J. Abdullah, Y. Sulaiman, I. Ibrahimb and N. M. Huang, *RSC Adv*., 6 (2016) 89430.
30. X. Cao, Y. Ye and S. Liu, *Anal. Biochem*. 1 (2011) 1.
31. Y. Hu, J. Jin, P. Wu, H. Zhang and C. Cai, *Electrochim. Acta*, 56 (2010) 491.
32. H. Zhao, X. Ji, B. Wang, N.Wang, X. Li and R. Ni, *Biosens. Bioelectron*., 65(2015) 23.
33. W. S. Hummers and R. E. Offeman, *J. Am. Chem. Soc*., 80 (1958) 1339.
34. T. Oritani, N. Fukuhara, T. Okajima, F. Kitamura and T. Ohsaka, *Norg. Chim. Acta.*, 357 (2004) 436.
35. H. Gampp and S.J. Lippard, *Inorg. Chem.* 22 (1983) 357.
36. S. Xue, H. Yi, Y. Yuan, P. Jing and W. Xu, *Anal Methods*, (2015) 1.
37. F. Valentini, L. Cristofanelli, M. Carbone and G. Palleschi, *Electrochim. Acta*, 63 (2012) 37.
38. J. Chen, U. Wollenberger, F. Lisdat, B. Ge and F. W. Scheller, *Sens. Actuators B*, 70 (2000) 115.
39. X. Wang, M. Han, J. Bao, W. Tu and Z. Dai, *Anal. Chim. Acta.*, 717 (2012) 61.
40. H. Zejli, J. L. H. H. de Cisneros, I. Naranjo-Rodríguez and K. R. Temsamani, J. L. Marty, *Talanta*, 80 (2010) 1805.
41. K. Thandavan, S. Gandhi, S. Sethuraman, J. B. B. Rayappan and U. M. Krishnan, *Sens. Actuators B*, 176 (2013) 884.
42. P. Santhosh, K. M. Manesh, S. Lee, S. Uthayakumar, A. I. Gopalana and K. P. Lee, *Analyst* 136 (2011) 1557.
43. Q. Ye, W. Li, Z. Wang, L. Zhang, X. Tan and Y. Tian, *J Electroanal Chem* 729 (2014) 21.

44. S. Peteu, T. Bose and M. Bayachou, *Anal. Chim. Acta*, 780 (2013) 81.